JACS
JOURNAL OF THE AMERICAN CHEMICAL SOCIETY

Article

pubs.acs.org/JACS

Negative Dielectrophoretic Capture and Repulsion of Single Cells at a Bipolar Electrode: The Impact of Faradaic Ion Enrichment and Depletion

Robbyn K. Anand, Eleanor S. Johnson, and Daniel T. Chiu*

Department of Chemistry, University of Washington, Seattle, Washington 98195, United States

Supporting Information

ABSTRACT: This paper describes the dielectrophoretic (DEP) forces generated by a bipolar electrode (BPE) in a microfluidic device and elucidates the impact of faradaic ion enrichment and depletion (FIE and FID) on electric field gradients. DEP technologies for manipulating biological cells provide several distinct advantages over other cell-handling techniques including label-free selectivity, inexpensive device components, and amenability to single-cell and array-based applications. However, extension to the array format is nontrivial, and DEP forces are notoriously short-range, limiting device dimensions and throughput. BPEs present an attractive option for DEP because of the ease with which they can be arrayed. Here, we present experimental results demonstrating both negative DEP (nDEP) attraction and repulsion of B-cells from each a BPE cathode and anode. The direction of nDEP force in each case was determined by whether the conditions for FIE or FID were chosen in the experimental design. We conclude that FIE and FID zones generated by BPEs can be exploited to shape and extend the electric field gradients that are responsible for DEP force.

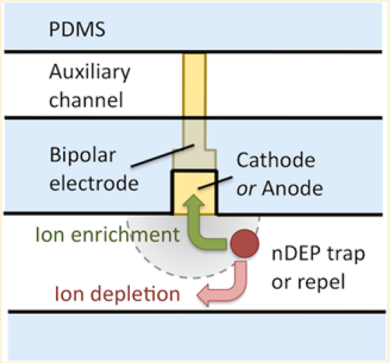

INTRODUCTION

We present a dielectrophoresis (DEP) technique that employs electric field gradients formed by localized faradaic ion enrichment and depletion (FIE and FID) zones at bipolar electrodes (BPEs) in a microfluidic device for the manipulation of a few or single cells. This technological development is significant because (1) it addresses a need for effective and inexpensive single-cell manipulation in microfluidic devices, (2) the FIE and FID zones provide electric field gradients having a tunable size and shape, and (3) the use of BPEs allows facile arraying.

Over the past decade, the scientific community has become increasingly attuned to heterogeneity in seemingly homogeneous cell populations. Even among clonal cells, stochastic events lead to variations in gene expression and diverse responses to endogenous and exogenous stimuli. Cellular heterogeneity has documented impact in many fields of research such as the rare induction of somatic cells into pluripotent stem cells,[1] division of labor in neighboring neurons,[2] and varied drug response.[3] Heterogeneity within cancer cell populations[4,5] is of special interest for cancer treatment strategies because a minority of drug resistant cells can seed cancer recurrence after 'clinical cure.' None of these processes can be studied effectively using ensemble measurements, and therefore, many highly sensitive analytical tools have been developed for probing single cells.[6,7]

An ongoing challenge in single-cell analysis is manipulation (e.g., transport, sorting, trapping, and filtering) of the cells of interest. DEP manipulation of cells has been used to accomplish all of these functions while maintaining a high degree of cell viability. DEP is especially attractive for several reasons. First, cells can often be distinguished without the addition of labels (e.g., magnetic particles or fluorophores) owing to polarizabilities unique to cellular phenotype, size, and viability.[8−11] Second, DEP devices are generally comprised of planar electrodes or insulating barriers made of sufficiently inexpensive components to allow the production of disposable devices, an especially desirable characteristic for medical diagnostics devices, for which cross-contamination must be avoided.[10] Third, DEP has been demonstrated to be useful for single cell manipulation.[12−14] This has been accomplished by constraining the trapping point either by adding physical barriers or by defining an electric field cage similar in size to a single cell. In either case, DEP conditions are chosen that prevent cell−cell attraction, thus discouraging multicell capture. Finally, DEP can be more easily operated in parallel versus some competing technologies such as optical tweezers[6] or purely fluidic systems, which require a network of pumps and valves.[6,15]

Despite these major advantages, current DEP technologies have remaining challenges to overcome, and three of the most serious shortcomings relate to the generation of the electric field gradient required for DEP force. First, while DEP technologies can be operated in parallel, there are practical barriers to achieving an array of local electric field gradients. There are two common ways of forming gradients in an applied electric field—namely, (1) by applying a nonuniform field with

Received: October 6, 2014
Published: January 6, 2015

DOI: 10.1021/ja5102689
J. Am. Chem. Soc. 2015, 137, 776−783

Scheme 1. Microfluidic Devices Comprising a Bipolar Electrode and Illustration of Overpotential (η)

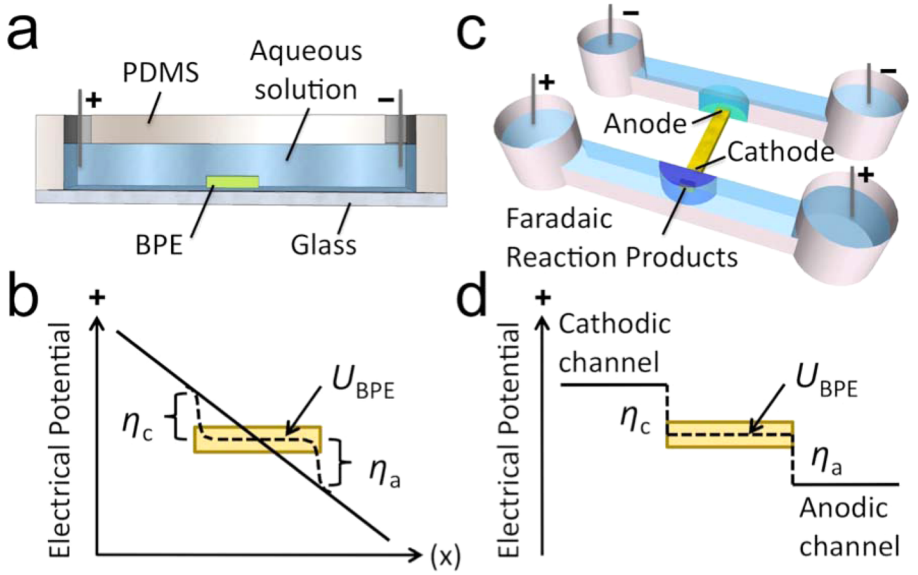

closely spaced electrodes and (2) by constraining the field with insulating barriers. Devices that form electric field gradients based on electrode arrays require the fabrication and actuation of many electrodes and wire leads—thereby leading to complex design and external instrumental control. Devices comprised of insulating barriers can only achieve precise trapping locations in positive DEP operating conditions, in which cells are trapped at vertices or constrictions where electric field maxima may be damaging to the cells.

Second, the range over which DEP force exists around these electrodes and insulating barriers can be too short for high-throughput device operation.[10,16] Specifically, significant field gradients are often effective over one to several cell diameters. This problem has been partially addressed by complex device fabrication techniques that implement 3D electrodes, including modification of microfluidic channel walls and ceiling.[10]

Third and finally, the shape of the electric field gradient produced by each of these strategies is fixed, lacking plasticity. One recently developed technology, optical DEP (or optoelectronic tweezers, OETs), has addressed this shortcoming through real-time light-based patterning of "virtual electrodes" in a semiconducting layer under a DEP chamber.[17,18] While OETs offer unprecedented spatial control over DEP force, the integration of OET materials and structures with existing microfluidic modalities is nontrivial.

Here, we employ BPEs to exert DEP force, and we modulate this force via the local conductivity of an aqueous medium.[19−23] This technique differs from medium conductivity gradient DEP, used to sort particles based on their conductivities,[24] in that, here, steeper gradients are locally and electrochemically generated, thus enabling them to contribute significantly to the DEP force experienced by cells near the BPE. As a result, cells are trapped or repelled by the resulting electric field gradients. Importantly, this technology addresses each of the challenges faced by existing DEP technology. First, BPEs can be operated in an array format without requiring wire leads (electrical contact) to each individual BPE.[25] As a result, the device is simple to fabricate. Second, the electric field gradients, which exert DEP force on the cells, have controllable size and can traverse the microchannel cross section. This feature is important because the device dimensions and throughput are not limited by short-range DEP forces. Finally, the shape of the electric field gradient can be tuned fluidically. In the following sections we describe the operating principles of the DEP at a BPE and describe initial results demonstrating the manipulation of cells.

THEORETICAL BACKGROUND

Bipolar Electrochemistry. Scheme 1a is an illustration of a bipolar electrode (BPE)—here, a planar strip of conducting material—in a microfluidic channel. When a DC voltage bias is applied across the fluidic channel, a linear potential profile develops (solid line, Scheme 1b). The potential of the BPE (U_{BPE}) floats to a value intermediate to the potential of the aqueous solution in contact with its ends. The potential difference (η) between the BPE and solution is a driving force for oxidation (η_a) and reduction (η_c) reactions at opposite ends of the BPE. Importantly, faradaic reactions are achieved at the BPE without direct electrical contact to the BPE, and this feature allows multiple BPEs to be operated in parallel. The rates of electron transfer to (oxidation) and from (reduction) the BPE are coupled and lead to a current through the BPE (i_{BPE}).[26] Note that when i_{BPE} is nonzero, it competes with ionic current in the microchannel and impacts the potential drop in solution as indicated by the dashed line in Scheme 1b.[27]

Generation of Faradaic Ion Enrichment and Depletion (FIE and FID) Zones. Faradaic electrochemistry at the BPE ends can perturb the electric field through the formation of FIE (high conductivity, low field strength) or FID (low conductivity, high field strength) zones. For example, an increase in local ionic strength at the anodic end of a BPE has been demonstrated to occur via water oxidation followed by Tris buffer protonation.[19]

$$4H_2O - 2e^- \rightarrow 2H_3O^+ + O_2 \quad (1)$$

$$Tris + H_3O^+ \rightarrow TrisH^+ + H_2O \quad (2)$$

Within the confinement of a microfluidic channel, this increased concentration of $TrisH^+$ cations can remain localized around the anodic end of the BPE. Anions will electromigrate to charge pair with these cations, forming an FIE zone.[19]

DOI: 10.1021/ja5102689
J. Am. Chem. Soc. 2015, 137, 776−783

Scheme 2. Principles of nDEP Repulsion and Capture at FID and FIE Zones near a BPE Tip

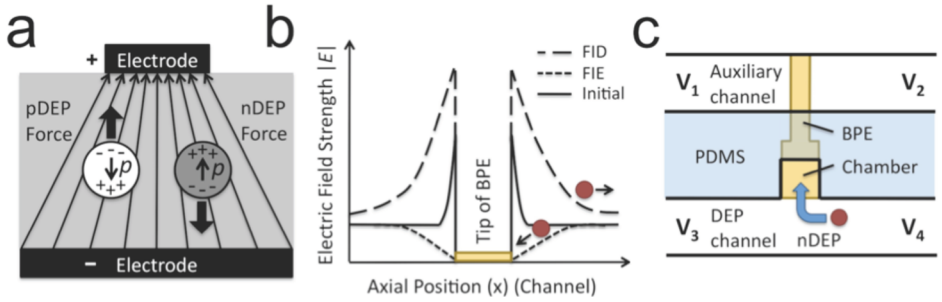

Importantly, any oxidation or reduction reaction adding charge to a solution-phase species can similarly lead to an accumulation of positively and negatively charged ions at *either* the BPE anode or cathode. Conversely, a decrease in local ionic strength at the cathodic end of a BPE has been demonstrated to occur via the following set of reactions.[19]

$$2H_2O + 2e^- \rightarrow 2OH^- + H_2 \quad (3)$$

$$TrisH^+ + OH^- \rightarrow Tris + H_2O \quad (4)$$

The net result of this series of reactions is the neutralization of the buffer cation, $TrisH^+$ to neutral Tris. In this case, the coanion (Cl^-) was shown to migrate away from the site of neutralization, thus leading to localized FID at the BPE cathode.[19] Likewise, the neutralization of any charged species can lead to formation of an FID zone. Importantly, the shape and position of the FIE and FID zones can be controlled using convection.[22]

Finally, these FIE and FID zones have been formed at BPE ends that are fluidically isolated as shown in Scheme 1c. In this case, the solution potential in contact with the BPE in the cathodic channel is higher than U_{BPE} and, in the anodic channel, is lower than U_{BPE} (Scheme 1d). Note that the solution potentials represented in Scheme 1d are for the solution directly above the BPE and do not represent the potential profile along the length of each microchannel. A key advantage of this device configuration is that the applied DC voltage required to drive faradaic processes is significantly lower than the case in the single channel design. This improvement is owed to the removal of an ionic current path (fluidic junction) between the anodic and cathodic driving electrodes. This dual channel system has been used for electrophoretic enrichment of charged species[19−23] and electrostatic repulsion-based desalination[28] in DC-only electric fields.

DEP Manipulation of Cells Using BPEs. Here, we utilize these FIE and FID zones for DEP attraction and repulsion of biological cells. The mechanism by which ion concentration impacts DEP force is described here briefly. A polarizable particle subjected to an electric field will develop an effective dipole moment, p (Scheme 2a).[9] The magnitude of the dipole depends upon the volume of the particle, its degree of polarizability, and the strength of the surrounding electric field (E). In the presence of an electric field gradient, the particle will be attracted to regions of higher $|E|$ if the complex permittivity of the particle (ε^*_p) is greater than the complex permittivity of the surrounding medium (ε^*_m). This condition is called positive DEP (pDEP). Conversely, negative DEP (nDEP) will occur if ε^*_p is less than ε^*_m. The magnitude of DEP force (F_{DEP}) exerted on a spherical particle is given by the following equation.

$$F_{DEP} = 2\pi r^3 \varepsilon_m \mathrm{Re}[K(\omega)] \nabla |E_{RMS}|^2 \quad (5)$$

Here, r is the particle radius and $\mathrm{Re}[K(\omega)]$ is the real part of the Clausius−Mossotti factor (K), which is a function of electric field frequency (ω).

$$K = (\varepsilon^*_p - \varepsilon^*_m)/(\varepsilon^*_p + 2\varepsilon^*_m) \quad (6)$$

$$\varepsilon^* = \varepsilon + \frac{i\sigma}{\omega} \quad (7)$$

Equations 5−7 highlight the dramatic impact that a local change in solution conductivity (σ) can have on F_{DEP}. Specifically, the formation of an FID zone leads to an ohmic increase in the local magnitude of E and, simultaneously, causes ε^*_m to decrease (making K more positive). Likewise, FIE can have the opposite effect on E and ε^*_m. This synergistic effect is important because, as a particle is attracted (for instance, by pDEP into a high $|E|$ region), the magnitude of K can increase, leading to amplified attraction.

The experimental results presented here demonstrate nDEP attraction and repulsion of B-cells to and from FIE and FID zones generated at a BPE in a microfluidic device. These conductivity gradients act as extensions to the BPE, thus impacting a larger volume than the electric field gradients surrounding a typical planar electrode. Scheme 2b (not to scale) illustrates the anticipated impact of FIE and FID on the axial component of the electric field adjacent to *either end* of a BPE in a microfluidic device (such as that depicted in Scheme 1c). This simplified depiction assumes that the driving voltage applied to the device is symmetrical about the BPE. At an active BPE (i.e., $i_{BPE} \neq 0$) the electric field is zero directly above the BPE and enhanced at the BPE edges (Scheme 2b, solid line). The formation of an FIE zone leads to an ohmic decrease in the local magnitude of E, with the greatest impact nearest the BPE. At the BPE, the electric field remains zero. A cell will be trapped by nDEP at the resulting electric field minimum, at which the cell has a reduced risk of electric field-induced damage. Conversely, FID leads to an increase in the local magnitude of E, leading to enhanced and extended nDEP repulsion of a cell from the BPE. Previous measurements and simulations of E have shown that an electric field gradient formed by FIE and FID can extend up to several hundred microns from the BPE.[19,21,22] Table 1 shows the estimated nDEP force experienced by 10 μm- and 20 μm-diameter cells at the field maxima of electric field gradients attainable by FIE and FID. As a point of reference, the drag force experienced by these cells moving through solution at 20 μm/s is 1.9 and 3.8 pN, respectively. Although stronger fields may be used in certain applications, the maximum field strengths shown here are limited by the threshold of the transmembrane potential for

DOI: 10.1021/ja5102689
J. Am. Chem. Soc. 2015, 137, 776−783

Table 1. Effect of Electric Field Gradient Length on F_{DEP} for a 30 kV/m−0 kV/m Gradient

	$F_{DEP\ max}$ (pN)	
gradient length (μm)	d = 10 μm	d = 20 μm
300	1.7	13.3
200	2.6	19.9
100	4.9	39.9
50	10.2	80.1

electroporation (approximately 0.5 V).[29] The exact threshold at which electroporation occurs is determined by the solution conditions (esp. conductivity), cell membrane characteristics, and pattern of the applied field. Given a threshold of U_{trans} = 0.5 V, E must be maintained below 33 kV/m for a 20 μm-diameter cell (or 66 kV/m for a 10 μm-diameter cell).

MATERIALS AND METHODS

Chemicals. The RPMI 1640 media employed for cell culture was purchased from American Type Culture Collection (ATCC) (Manassas, VA). Ethylene glycol-propylene glycol block copolymer (Pluronic F108), bovine serum albumin (BSA) (≥98% purity), and 1.0 M Tris·HCl stock solution were obtained from Sigma-Aldrich, Inc. (St. Louis, MO). The silicone elastomer and curing agent (Sylgard 184) used to prepare the poly(dimethylsiloxane) (PDMS) microfluidic devices were obtained from K. R. Anderson, Inc. (Morgan Hill, CA). All other chemicals were reagent grade and purchased from Fisher Scientific (Thermo Fisher Scientific, Inc., Waltham, MA) including sodium phosphate (mono- and dibasic), sucrose, and dextrose (D-glucose). All dilutions were carried out with Milli-Q water (18.0 MΩ·cm). DEP buffers were comprised of 8.0% sucrose, 0.3% dextrose, and 0.1% BSA in either 10 mM Tris (pH 8.1) or 10 mM phosphate (pH 7.2) buffer.

Cell Culture. Mouse pro-B BaF3 B-cells were obtained from ATCC. These B-cells were cultured in RPMI 1640 supplemented with 1% pen-strep and 10% fetal bovine serum at 37 °C and 5% CO_2. The cells were subcultured every 3−4 days such that the concentration of cells did not exceed 1 × 10^6 cells/mL. In preparation for DEP experiments, ∼1 × 10^6 cells were pelleted by centrifugation followed by resuspension in 5 mL of the desired DEP buffer. This process was repeated one additional time to ensure cell culture medium components were removed.

Device Fabrication. PDMS/glass hybrid microfluidic devices with embedded Au BPEs were fabricated using standard photolithographic techniques.[30] Briefly, 1-mm-thick glass slides coated with 100 nm Au (no binding layer) were photolithographically patterned using SPR220-7.0 photoresist followed by wet-etching the Au in a 10% KI and 2.5% I_2 solution. The remaining photoresist was then dissolved with acetone. PDMS microchannels were molded by pouring precursor onto an SU-8 master and curing at 70 °C for 2 h. Reservoirs with 4-mm diameters were punched at both ends of each microchannel. The PDMS and Au-on-glass substrates were aligned and irreversibly sealed by the following process. First, both substrates were exposed to an O_2 plasma (plasma cleaner, Harrick Scientific, Ithaca, NY) for 1 min. Second, a drop of ethanol was applied to the glass substrate. Third, the PDMS monolith was put in contact with the glass substrate and aligned under a microscope. Then, the device was baked at 70 °C for 1 h to drive off ethanol. Finally, the device was filled with 3 μM Pluronic in either 10 mM Tris (pH 8.0) or 10 mM phosphate (pH 7.2) buffer selected to match the type of DEP buffer to be employed. The device was covered with parafilm and incubated at 4 °C overnight (at least 18 h). Pluronic coating served to dampen electroosmotic flow.[31]

The device dimensions were as follows. Dual parallel microchannels were each 4.0 mm long × 20 μm tall × 60 μm wide and separated by 400 μm. The channel inlets were tapered with a 53° angle leading to 4.0-mm-diameter reservoirs. The ceiling of the inlets was supported with diamond-shaped pillars (100 μm × 40 μm). This inlet geometry was designed to facilitate unimpeded introduction of cells into the microchannels. At the center of one microchannel (the DEP channel, Scheme 2c), there was a 30 μm × 30 μm side chamber, which was aligned to the BPE tip. The exposed BPE tip was approximately 30 μm wide × 30 μm long (defined by chamber). The auxiliary end of the BPE extended across the auxiliary channel (Scheme 2c) and was 15 μm wide.

DEP Experiments. The combined AC/DC electric field was applied to four Pt wires dipped in the device reservoirs (V_1, V_2, V_3, V_4, Scheme 2c) using a Hewlett-Packard 33120A waveform generator (Hewlett-Packard, Palo Alto, CA) and Kepco Model BOP 1000 M amplifier (Kepco, Inc., Flushing, NY). The AC field frequency was maintained at 1.8 kHz, at which the Clausius−Mossotti factor is −0.5 (maximum nDEP force) for B-cells under the conditions employed here. Prior to a DEP experiment, each microfluidic channel was rinsed with the appropriate DEP buffer (as indicated in the Results and Discussion section) for 1 min at 3 psi. The reservoirs were then filled with DEP buffer containing 2 × 10^5 B-cells/mL. Where indicated in the Results and Discussion section, cell viability was tested by exposing DEP-trapped cells to 0.4% Trypan blue dye in DEP buffer for >5 min.

RESULTS AND DISCUSSION

In this section, we describe nDEP attraction and repulsion of cells from a BPE and the impact of FIE and FID on these forces. We demonstrate nDEP repulsion of B-cells from a BPE in the absence of faradaic reactions (i.e., no DC field component). We then show that FIE at either the BPE anode or cathode leads to nDEP attraction that increases with increased AC field strength. These results are contrasted with nDEP repulsion of B-cells from an FID zone.

nDEP at a BPE in the Absence of Faradaic Reactions. Figure 1a demonstrates that a B-cell undergoes nDEP repulsion from a BPE tip in an AC-only electric field. In this experiment, the DEP channel (Scheme 2c) was rinsed with DEP buffer (8.0% sucrose, 0.3% dextrose, and 0.1% BSA in 10 mM Tris (pH 8.0)), and then, it was filled with the same DEP buffer containing 2 × 10^6 B-cells/mL. The auxiliary channel was rinsed and filled with 10 mM NaCl as an electrolyte.

Flow (right to left, Figure 1a) was established in the DEP channel by introducing a solution height differential in the reservoirs at its ends such that the average linear flow velocity ν_{avg} = 20 μm/s. An AC voltage of 64 Vpp at 1.8 kHz was applied to the left-hand reservoir of the DEP channel (V_3, Scheme 2c), and the remaining three reservoirs were grounded. Under these conditions, the spatially averaged root-mean-square (RMS) electric field strength along the DEP channel was $E_{RMS,avg}$ = 5.7 kV/m. As the cell approached the BPE, $E_{RMS,avg}$ was increased stepwise (from 1 V peak-to-peak (Vpp) to 6 Vpp on the waveform generator at 1 Vpp per second) from 5.7 kV/m at t = 0 s (slice 1) to 17.7 kV/m at t = 5 s (slice 3). The cell was briefly attracted toward the BPE and then repelled by nDEP from the locally high electric field around the BPE tip. The greatest deflection (between slices 2 and 3) is 20 μm over 2.5 s, which requires ∼1 pN of force. This result is significant because it establishes (1) that these AC field strengths are sufficient to exert nDEP force and (2) the electric field strength around the BPE is a local maximum in the absence of faradaic current and FIE. These results are corroborated by numerical simulations of F_{DEP}, in which i_{BPE} = 0 and $E_{RMS,avg}$ = 25 kV/m. Figure 1b shows the simulated y-component of F_{DEP} ($F_{DEP,y}$) surrounding the BPE in the xy-plane located at z = 5 μm above the BPE and channel floor. Negative values of $F_{DEP,y}$ indicate nDEP repulsion (in the negative direction on the y-axis). The magnitude of $F_{DEP,y}$ ranges from −320 pN to 760 pN. However, several cell diameters from the BPE, $F_{DEP,y}$ is nearer to 10 pN,

DOI: 10.1021/ja5102689
J. Am. Chem. Soc. 2015, 137, 776−783

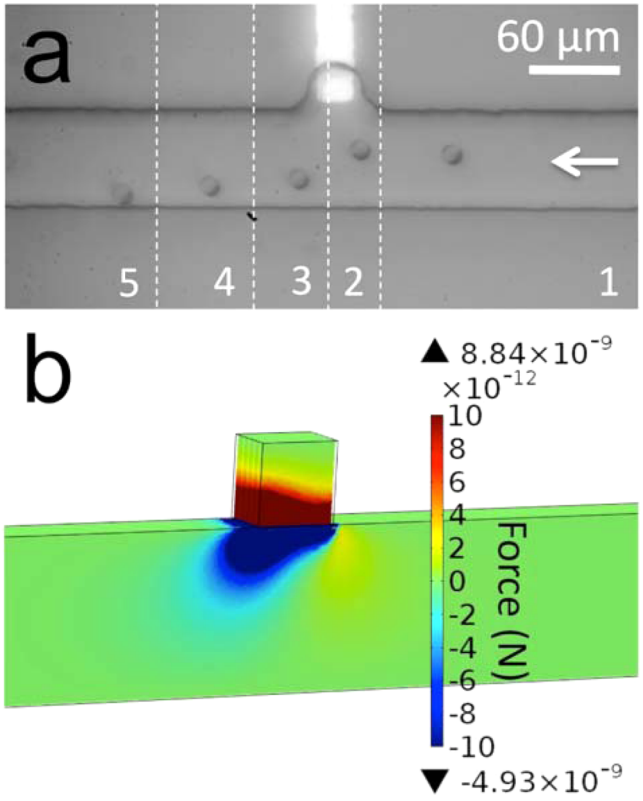

Figure 1. (a) A series of optical micrographs, which show nDEP repulsion of a B-cell from the BPE tip under AC-only electric field in Tris DEP buffer. Each image slice (numbered sequentially 1−5) is separated by 2.5 s. $E_{RMS,avg}$ = 5.7 kV/m (t = 0 s) to 17.7 kV/m (t = 5 s). (b) Simulated magnitude of the y-component of F_{DEP} in the xy-plane at z = 5 μm.

which is consistent with typical F_{DEP} magnitudes 10−20 μm from an electrode surface.[32,33] At the channel midline, F_{DEP} has decreased to <2 pN. Details of the simulation are included in the Supporting Information (SI). Most importantly, the simulation correctly predicts the trajectory of the B-cell as it traverses the channel from right to left. There is weak (several pN) attraction of the cell (positive y-direction) to the right of the BPE followed by further-reaching repulsive forces.

nDEP Attraction of a B-Cell to an FIE Zone at the BPE Anode and the BPE Cathode. In the previous subsection, we established that an AC field alone results in nDEP repulsion of B-cells from the BPE tip. Here, we demonstrate nDEP attraction to the BPE with the addition of a DC offset. The DC field can drive faradaic current (i_{BPE}) leading to an FIE zone at either a BPE anode or a BPE cathode. Due to the negative charge of the cell membrane, in these two cases DEP force works with and against electrophoretic (EP) force, respectively. First, we will examine nDEP attraction of a B-cell to an FIE zone at the *BPE anode* in Tris DEP buffer (Figure 2a−2c). In this device, nDEP cell trapping proceeded at the BPE anode as follows. First, the channels were rinsed and filled as described in the previous subsection. Then, flow was established as before such that v_{avg} = 65 μm/s. An AC field with a *negative* DC offset was applied at V_3 versus ground (V_1, V_2, and V_4) such that $E_{RMS,avg}$ = 5.7 kV/m AC and $E_{DC,avg}$ = 0.75 kV/m DC. Figure 2a shows the resulting cell trajectory in 1 s slices. Under these conditions, the EP force exerted by the BPE anode was insufficient to attract and trap the B-cells. However,

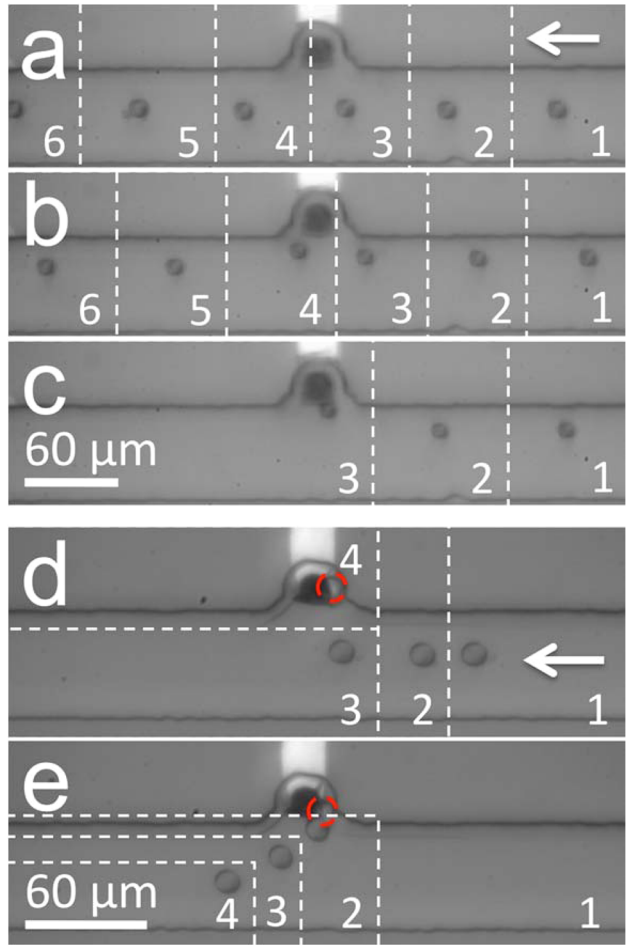

Figure 2. (a−c) Multiple series of optical micrographs showing increasing nDEP attraction of a B-cell toward the BPE anode in Tris DEP buffer. $E_{DC,avg}$ = 0.75 kV/m, $E_{RMS,avg}$ for (a) 5.7 kV/m, (b) 13.3 kV/m, (c) 17.7 kV/m. Image slices are 1 s apart. (d) nDEP attraction of a B-cell toward the BPE cathode in phosphate DEP buffer (4 s/slice). $E_{DC,avg}$ = 1.5 kV/m, $E_{RMS,avg}$ increased from 5.7 kV/m to 28.3 kV/m from t = 0 s (slice 1) to t = 8 s (slice 3). (e) Release of the trapped cell (2 s/slice) from (d) upon subsequent decrease of $E_{RMS,avg}$ to 5.7 kV/m (from slice 1 to slice 2).

as the AC field strength was increased (Figure 2a−2c; $E_{RMS,avg}$ = 5.7, 13.3, and 17.7 kV/m, respectively) cells were increasingly attracted and finally trapped. This finding is significant because nDEP attraction toward the BPE indicates that the electric field is depressed around the BPE by FIE. At later time points than those displayed in Figure 2c, the trapped cell was pulled into the microchamber and remained over the BPE.

This result is attributed to an averaged axial electric field profile like that shown in Scheme 2b (dashed line indicating "FIE") caused by the progression of the oxidation reaction described by eq 1 leading to the accumulation of ionic species around the BPE. This ion enrichment zone decreases E locally. Importantly, although E is zero above the BPE whenever i_{BPE} is nonzero (solid and dashed lines, Scheme 2b), cells can only be attracted to this region after an FIE zone forms. In a control experiment, many cells were trapped under similar trapping conditions but on a larger area BPE, which extended across the DEP channel. These cells were tested for viability by flowing 0.4% Trypan blue in DEP buffer for >5 min. The cells did not uptake Trypan blue, thus indicating intact membrane integrity and viability. However, cells exposed to more positive or

DOI: 10.1021/ja5102689
J. Am. Chem. Soc. 2015, 137, 776−783

negative DC voltages after trapping but before exposure to Trypan dye were stained blue, indicating membrane degradation.

Likewise, we carried out nDEP trapping of a B-cell at the BPE *cathode* (Figure 2e−2d and SI Movie 1). In this case, a similar device was filled with 10 mM phosphate (pH 7.2) in 8% sucrose, 0.3% dextrose, and 0.1% BSA (phosphate DEP buffer). An AC field with a *positive* DC offset was applied at V_3 such that $E_{RMS,avg}$ = 5.7 kV/m AC and $E_{DC,avg}$ = 1.5 kV/m DC. Water reduction followed by deprotonation of phosphate species led to ion enrichment around the BPE tip. As the AC field strength was increased gradually from 5.7 kV/m to 28.3 kV/m, the cell was pulled into the chamber by nDEP (Figure 2d, 4 s/slice), and as the AC field was returned to 5.7 kV/m, the cell was expelled from the chamber (Figure 2e, 2 s/slice). This result is significant for two reasons. First, as in the previous experiment, this result demonstrates that faradaic current leading to FIE sufficiently decreases the local electric field around the BPE to reverse the role of nDEP from repulsion to attraction. Second, in this case, the cell was trapped by nDEP force despite electrostatic repulsion of the negatively charged cell from the BPE cathode. The role of EP is underscored by the immediate expulsion of the cell from the chamber once the AC field strength was decreased (Figure 2e). In both of these cases, F_{DEP} ranges from 1 to 3 pN, which is similar in magnitude to the control of Figure 1a (no FIE) but with a reversed sign. Here, the force is weak because the electric field gradient is formed based on a decrease in local field strength, and both the magnitude and slope of the field contribute to F_{DEP}.

This result has been repeated with the BPE misaligned from the chamber such that the two features are laterally separated by 50 μm and the BPE extends 15 μm into the channel (results not shown). In this control experiment, regardless of the direction of flow, cells favored trapping at the BPE rather than the chamber. This result verifies that the zero electric field directly above the BPE and FIE depression of the surrounding field are the primary mechanisms responsible for cell trapping.

Furthermore, we performed a control with no BPE (results not shown). While the electric field in an empty chamber (no BPE) is lower than that in the microchannel, at AC field strengths up to E_{avg} = 28.3 kV/m, cells are only weakly attracted to the chamber and are only drawn into it under stopped-flow conditions.

nDEP Repulsion of a B-Cell from an FID Zone. Just as crucial as an understanding of the impact of FIE on F_{DEP} is an examination of the FID regime. The enhanced local electric field strength associated with ion depletion can lead to enhanced EP exclusion of particles, thus, complicating the delineation of DEP and EP forces in the FID zone. To separately interrogate the role of nDEP in cell repulsion from an FID zone, we once again increased the AC field contribution while maintaining a constant DC component. In this experiment, the device was prepared with 10 mM Tris DEP buffer (DEP channel) and 10 mM NaCl (auxiliary channel) as described in previous subsections. A flow rate of ν_{avg} = 85 μm/s (left to right) was established in the channel. An AC field with a *positive* DC offset was applied at V_3 such that $E_{RMS,avg}$ = 0.57 kV/m and $E_{DC,avg}$ = 1.25 kV/m DC. Water reduction at the BPE cathode followed by neutralization of $TrisH^+$ ions (eqs 3 and 4) led to ion depletion around the BPE tip. Figure 3a−3d (0.5 s/slice, SI Movie 2) show increasing degrees of nDEP repulsion of a B-cell from the resulting FID zone as the AC field strength was increased from $E_{RMS,avg}$ = 0.57 kV/m to 6.13, 7.95, and then 10.25 kV/m, respectively. The DEP force exerted on the ∼12-μm-diameter cells at the greatest measured deflection (between 0.5-s slices) was estimated as 1.2, 4.7, 6.6, and 7.6 pN, respectively. The force gained an ∼0.7 pN per 1 kV/m increase in $E_{RMS,avg}$ over this range. The key point is that by simply changing the identity of the DEP buffer from phosphate, which creates an FIE zone in the presence of OH^-, to Tris, which is neutralized under the same conditions, cells go from being pulled into the chamber (Figure 2d) to colliding with the opposing channel wall (Figure 3d). Furthermore, we have demonstrated that the causative force is dielectrophoretic. nDEP repulsion of cells from an FID zone formed at the BPE *anode* in phosphate DEP buffer was also performed (see SI Figure S1).

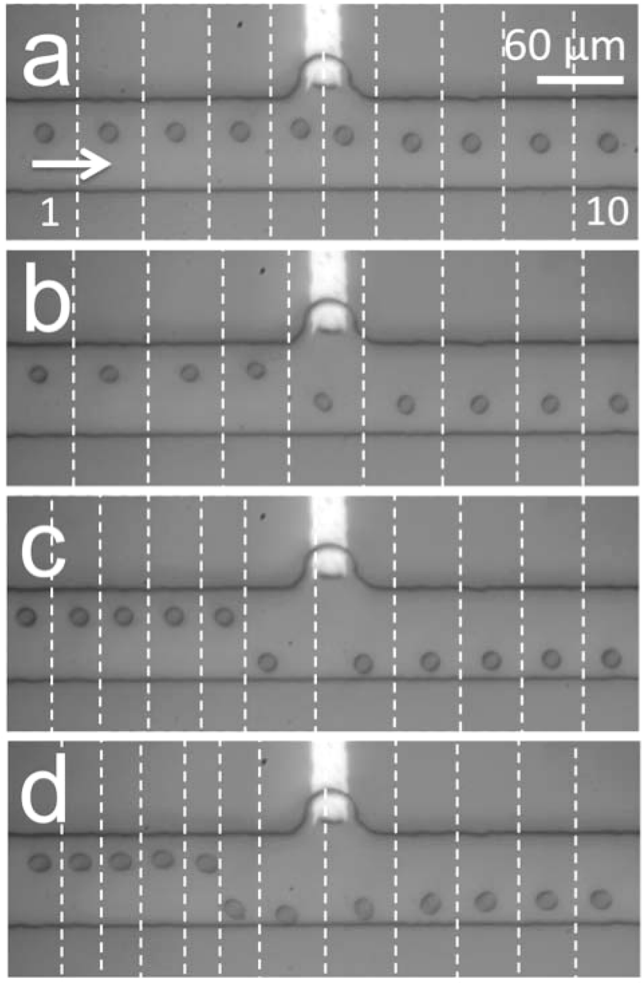

Figure 3. (a−d) Multiple series of optical micrographs, which demonstrate nDEP repulsion of individual B-cells from an FID zone at the BPE cathode in Tris DEP buffer (0.5 s/slice). $E_{DC,avg}$ = 1.25 kV/m. $E_{RMS,avg}$ is (a) 0.57 kV/m, (b) 6.13 kV/m, (c) 7.95 kV/m, and (d) 10.25 kV/m.

In the experiment described in the above paragraph, the flow rate and faradaic reaction rate were selected such that cells could circumvent the FID zone. Figure 4a and 4b show cells repelled by a stronger and larger FID zone ($E_{DC,avg}$ = 2.5 kV/m) at the same flow rate (85 μm/s left to right) as was employed in Figure 3a−3d. It is important to note that EP repulsion of the negatively charged cells by the enhanced local electric field around the BPE cathode likely plays a significant role at this DC field strength. At low AC field strength ($E_{RMS,avg}$

DOI: 10.1021/ja5102689
J. Am. Chem. Soc. 2015, 137, 776−783

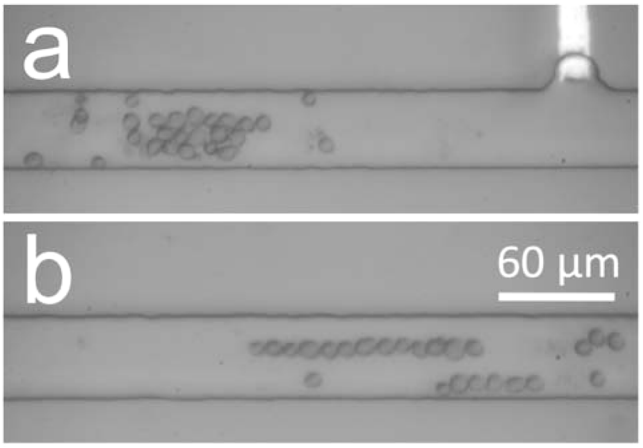

Figure 4. Sequential optical micrographs showing nDEP and EP repulsion of B-cells from an FID zone at the BPE cathode in Tris DEP buffer ($E_{DC,avg}$ = 2.5 kV/m) with $E_{RMS,avg}$ of (a) 0.57 kV/m and (b) 10.25 kV/m.

= 0.57 kV/m, Figure 4a), cells were impeded and accumulated along the electric field gradient formed by the FID zone where the force of electrophoresis and opposing fluid flow on the cells balanced (approximately 9.5 pN). We have also observed this effect with a DC-only field (SI Movie 3). When the AC field was subsequently increased to $E_{RMS,avg}$ = 10.25 kV/m, the additional nDEP force transported the cells to a new balance point >450 μm from the BPE (Figure 4b, image shifted 450 μm to the left versus Figure 4a). Pearl chaining was observed under these conditions due to the high AC field strength and fixed location of the cells. Importantly, the FID zone extends the reach of DEP force to several hundred microns from the BPE. Given a larger channel width, we anticipate that cells would be able to circumvent the large FID zone, albeit at several hundred microns from the BPE. These results also demonstrate the many roles of the DC field component: activation of the BPE ($i_{BPE} \neq 0$), control of FIE/FID zone size, and EP force. Therefore, the strength of the DC field is critical to DEP outcomes in a BPE-based device.

CONCLUSION

In conclusion, we have demonstrated both nDEP attraction and repulsion of biological cells from each a BPE cathode and anode including single cell sequestration in a side chamber. Furthermore, we have shown that the direction, magnitude, and extent of nDEP force can be controlled via faradaic reactions at the BPE, which impact the local conductivity of the DEP medium through the formation of FIE and FID zones. Numerical simulations quantifying the contribution of FIE and FID are in progress.

As a natural extension of this work, we are investigating several BPE array formats for array-based single-cell trapping and isolation. This technology will provide a powerful tool for parallel single-cell analysis. Additionally, we aim to exploit the selectivity of DEP for individual cell types. We anticipate that, at an AC frequency that produces distinct values of F_{DEP}, repulsion of cells from an extended FID zone will yield high-throughput sorting. Finally, these principles will extend to the pDEP regime (higher AC field frequencies) at which higher DEP forces will result due to a maximum value of the real part of the Clausius–Mossotti factor ($\mathrm{Re}[K(\omega)] = 1$).

ASSOCIATED CONTENT

Supporting Information

Movies 1, 2, and 3 (4× real time). Details of the simulation of nDEP repulsive forces around a BPE tip (Figure 1b). Additional experimental data demonstrating nDEP repulsion of cells from an FID zone formed at the BPE anode in phosphate DEP buffer (Figure S1). This material is available free of charge via the Internet at http://pubs.acs.org.

AUTHOR INFORMATION

Corresponding Author

*chiu@chem.washington.edu

Notes

The authors declare no competing financial interest.

ACKNOWLEDGMENTS

We thank Prof. Allen J. Bard for critical discussions regarding this work. We are grateful to the Department of Defense CDMRP Program (BC100510) for support of this work. R.K.A. was supported in part by Grant T32CA138312 from the National Cancer Institute. The content is solely the responsibility of the authors and does not necessarily represent the official views of the National Cancer Institute or the National Institute of Health.

REFERENCES

(1) Buganim, Y.; Faddah, D. A.; Jaenisch, R. *Nat. Rev. Genet.* **2013**, *14*, 427–439.
(2) Rubakhin, S. S.; Lanni, E. J.; Sweedler, J. V. *Curr. Opin. Biotechnol.* **2013**, *24*, 95–104.
(3) Kovarik, M. L.; Shah, P. K.; Armistead, P. M.; Allbritton, N. L. *Anal. Chem.* **2013**, *85*, 4991–4997.
(4) Marjanovic, N. D.; Weinberg, R. A.; Chaffer, C. L. *Clin. Chem.* **2013**, *59*, 168–179.
(5) Swanton, C. *Cancer Res.* **2012**, *72*, 4875–4882.
(6) Walling, M. A.; Shepard, J. R. *Chem. Soc. Rev.* **2011**, *40*, 4049–4076.
(7) Lecault, V.; White, A. K.; Singhal, A.; Hansen, C. L. *Curr. Opin. Chem. Biol.* **2012**, *16*, 381–390.
(8) Çetin, B.; Li, D. *Electrophoresis* **2011**, *32*, 2410–2427.
(9) Gagnon, Z. R. *Electrophoresis* **2011**, *32*, 2466–2487.
(10) Martinez-Duarte, R. *Electrophoresis* **2012**, *33*, 3110–3132.
(11) Shafiee, H.; Sano, M. B.; Henslee, E. A.; Caldwell, J. L.; Davalos, R. V. *Lab Chip* **2010**, *10*, 438–445.
(12) Sankaran, B.; Racic, M.; Tona, A.; Rao, M. V.; Gaitan, M.; Forry, S. P. *Electrophoresis* **2008**, *29*, 5047–5054.
(13) Taff, B. M.; Voldman, J. *Anal. Chem.* **2005**, *77*, 7976–7983.
(14) Faenza, A.; Bocchi, M.; Duqi, E.; Giulianelli, L.; Pecorari, N.; Rambelli, L.; Guerrieri, R. *Anal. Chem.* **2013**, *85*, 3446–3453.
(15) Kalisky, T.; Blainey, P.; Quake, S. R. *Annu. Rev. Genet.* **2011**, *45*, 431–45.
(16) Martinez-Duarte, R.; Renaud, P.; Madou, M. J. *Electrophoresis* **2011**, *32*, 2385–2392.
(17) Huang, K. W.; Wu, Y. C.; Lee, J. A.; Chiou, P. Y. *Lab Chip* **2013**, *13*, 3721–3727.
(18) Valley, J. K.; Neale, S.; Hsu, H. Y.; Ohta, A. T.; Jamshidi, A.; Wu, M. C. *Lab Chip* **2009**, *9*, 1714–1720.
(19) Hlushkou, D.; Perdue, R. K.; Dhopeshwarkar, R.; Crooks, R. M.; Tallarek, U. *Lab Chip* **2009**, *9*, 1903–1913.
(20) Laws, D. R.; Hlushkou, D.; Perdue, R. K.; Tallarek, U.; Crooks, R. M. *Anal. Chem.* **2009**, *81*, 8923–8929.
(21) Perdue, R. K.; Laws, D. R.; Hlushkou, D.; Tallarek, U.; Crooks, R. M. *Anal. Chem.* **2009**, *81*, 10149–10155.
(22) Anand, R. K.; Sheridan, E.; Hlushkou, D.; Tallarek, U.; Crooks, R. M. *Lab Chip* **2011**, *11*, 518–527.

DOI: 10.1021/ja5102689
J. Am. Chem. Soc. 2015, 137, 776–783

(23) Anand, R. K.; Sheridan, E.; Knust, K.; Crooks, R. M. *Anal. Chem.* **2011**, *83*, 2351−2358.
(24) Khoshmanesh, K.; Nahavandi, S.; Baratchi, S.; Mitchell, A.; Kalantar-zadeh, K. *Biosens. Bioelectron.* **2011**, *26*, 1800−1814.
(25) Chow, K. F.; Mavré, F.; Crooks, J. A.; Chang, B.-Y.; Crooks, R. M. *J. Am. Chem. Soc.* **2009**, *131*, 8364−8365.
(26) Mavré, F.; Anand, R. K.; Laws, D. R.; Chow, K. F.; Chang, B.-Y.; Crooks, J. A.; Crooks, R. M. *Anal. Chem.* **2010**, *82*, 8766−8774.
(27) Mavré, F.; Chow, K. F.; Sheridan, E.; Chang, B.-Y.; Crooks, J. A.; Crooks, R. M. *Anal. Chem.* **2009**, *81*, 6218−6225.
(28) Knust, K. N.; Hlushkou, D.; Anand, R. K.; Tallarek, U.; Crooks, R. M. *Angew. Chem., Int. Ed.* **2013**, *52*, 8107−8110.
(29) Somiari, S.; Glasspool-Malone, J.; Drabick, J. J.; Gilbert, R. A.; Heller, R.; Jaroszeski, M. J.; Malone, R. W. *Mol. Ther.* **2000**, *2*, 178−187.
(30) McDonald, J. C.; Duffy, D. C.; Anderson, J. R.; Chiu, D. T.; Wu, H.; Schueller, O. J. A.; Whitesides, G. M. *Electrophoresis* **2000**, *21*, 27−40.
(31) Hellmich, W.; Regtmeier, J.; Duong, T. T.; Ros, R.; Anselmetti, D.; Ros, A. *Langmuir* **2005**, *21*, 7551−7557.
(32) Wikland, M.; Günther, C.; Lemor, R.; Jäger, M.; Fuhr, G.; Hertz, H. M. *Lab Chip* **2006**, *6*, 1537−1544.
(33) Lvovich, V. F. *Impedance Spectroscopy Applications to Electrochemical and Dielectric Phenomena*; John Wiley & Sons: Hoboken, NJ, 2012; pp 138−139.

DOI: 10.1021/ja5102689
J. Am. Chem. Soc. 2015, 137, 776−783